



Analysis of light scattering by erythrocyte based on discrete sources method

Elena Eremina ^{a,*}, Yuri Eremin ^b, Thomas Wriedt ^c

^a *Universität Bremen, Badgasteiner Str. 3, 28359 Bremen, Germany*

^b *Faculty of Applied Mathematics and Computer Science, Moscow State University, Lenins Hills, 119992 Moscow, Russia*

^c *Institut für Werkstofftechnik, Badgasteiner Str. 3, 28359 Bremen, Germany*

Received 18 May 2004; received in revised form 17 July 2004; accepted 6 September 2004

Abstract

A renewed algorithm of the discrete sources method (DSM) is applied to model light scattering from a human erythrocyte. In contrast to traditional volume-based methods which are widely used for light scattering simulation DSM allows calculation of scattering for all incident angles and polarizations at once. This leads to an essential reduction of the computing time. The renewed DSM algorithm allows using a lower number of elementary sources which results in an increased accuracy of approximation for every harmonic. In this paper, we investigate several erythrocyte shapes such as flat spheroid and disk-sphere, which are usually used to represent the erythrocyte shape in light scattering modeling. Besides conventional mathematical shapes the rigorous biconcave erythrocyte shape was investigated. This is the first attempt to apply a semi-analytical method to model obstacle with concavities. Numerical results for light scattering by different shape models are presented and compared with the rigorous erythrocyte shape. Some practical recommendations in using appropriate models are given.

© 2004 Published by Elsevier B.V.

Keywords: Light scattering; Discrete sources method; Erythrocyte

1. Introduction

In recent years interest associated with polarized light scattering by different biological objects increased. Because biological structures are complex, it is generally difficult to study light scattering from a single object, however there are important exceptions, the blood cells. For experimental

* Corresponding author. Tel.: +49 421 218 3583; fax: +49 421 218 5378.

E-mail addresses: eremina@iwt.uni-bremen.de (E. Eremina), thw@iwt.uni-bremen.de (T. Wriedt).

studies of blood cells, the scanning flow cytometer (SFC) can be used. SFC is designed to measure the light-scattering pattern of individual particles [1,2]. The interaction of light and blood cells or tissue is important for different applications, e.g., the determination of hemoglobin and volume of red blood cells (erythrocytes), to improve differentiations of blood cells by physical means, the determination of oxygen concentration in tissue and the interpretation of images in optical mammography. The interested reader can obtain more information on the interaction of light and tissue in the papers by Tuchin [3] and Roggan [4]. Among other blood cells the erythrocyte is very important because of its hemoglobin content. In addition, human erythrocytes do not show internal structure, providing an opportunity to apply theoretical models of scattering to these cells. However, theoretical modeling of erythrocytes is still complicated, because of its shape, size and optical properties. The refractive index of an erythrocyte relative to blood plasma belongs to the range $1.045 \leq m \leq 1.058$, that means that for a scattering problem, where the incident light is a visible laser beam, an erythrocyte is a low-contrast dielectric scatterer. The size parameter band for blood cells is rather wide: from 26 until 50, the erythrocyte itself has a size parameter of 42, which makes modeling quite time-consuming. Another feature we should take into account is the complex shape of a real erythrocyte [2], which can change from biconcave discoid to a toroidal shape, due to the functions which an erythrocyte has in human blood. Recently, different methods have been applied to model light scattering from a single erythrocyte: Wentzel–Kramer–Brillouin approximation [5], Mie theory, Fraunhofer and anomalous diffraction [6], Rayleigh and Rayleigh–Gans–Debye approximation [7], Fredholm Integral Method, Boundary Integral Equation Method [8], T-matrix [9], Discrete Dipole Approximation (DDA) [10], Boundary Element Method (BEM) [11] and others. To model the erythrocyte shape, one usually uses the model of an oblate spheroid with aspect ratio 1:4 or even an equivolume sphere. The first attempt to solve scattering problem for real erythrocyte shape numerically has been made by Tsinopoulos and Polyzos [11].

In experimental studies SFC allows to measure light scattering from a single particle in angular range over $10\text{--}60^\circ$. The most interesting are two directions of scattering: forward scattered and side-scattered. The first one depends on particle size and the second on internal particle structure. Results obtained using SFC allow comparison of the results of theoretical modeling with the experimental results [2,10].

In this paper, the Discrete Sources Method [12] is applied to modeling light scattering from the human erythrocyte. In the frame of DSM, the approximate solution is constructed as a finite linear combination of the fields of Discrete Sources (DS): dipoles and multipoles deposited in some supplementary domain (axis of the symmetry of imaginary plane). The representation for the approximate solution satisfies all the conditions of the boundary value scattering problem, except conditions at the obstacle boundary. The unknown amplitudes of DS are to be determined from the transmission conditions at the obstacle boundary. So, the boundary value scattering problem under investigation is reduced to the solution of an approximation problem enforced at an obstacle surface [13]. Unlike volume-based methods like DDA and FDTD, the surface-based methods like DSM or T-matrix allow to compute scattering for all the incident angles and polarizations at once. In DSM only the surface of the scatterer has to be discretized. In addition taking into account of the rotational symmetry of the erythrocyte in DSM gives an essential reduction of calculation time compared with volume discretization methods.

To our knowledge, the paper presents the first attempt to apply a semi-analytical method to model obstacle with concavities. On the base of DSM a rigorous biconcave erythrocyte shape in parallel with such common mathematical shapes, like oblate spheroid and disk-sphere is modeled.

First we will present the mathematical theory of DSM. Next we will give an overview of numerical algorithm realization and present some numerical results for different erythrocyte shapes with detailed discussion. Conclusions and recommendations in using appropriate erythrocyte models are given at the end of the paper.

2. Mathematical model

Let us start with the mathematical statement of the scattering problem. We will consider scattering in an isotropic homogeneous medium in R^3 of an electromagnetic wave by a local homogeneous penetrable obstacle D_i with the smooth boundary ∂D . We use a cylindrical coordinate system (z, θ, φ) , z is also an axis of symmetry of a particle, θ_i is an incident angle with respect to z .

We assume the time dependence to be $\exp(j\omega t)$. Scattering is described by the electromagnetic fields $\{\mathbf{E}_\xi, \mathbf{H}_\xi\}$ satisfying Maxwell equations:

$$\begin{aligned} \nabla \times \mathbf{H}_{e,i} &= jk\varepsilon_{e,i}\mathbf{E}_{e,i}, \\ \nabla \times \mathbf{E}_{e,i} &= -jk\mu_{e,i}\mathbf{H}_{e,i}, \end{aligned} \quad \text{in } D_{e,i}, \quad D_e := R^3/\bar{D}_i, \quad (1)$$

the boundary condition enforced on the particle surface:

$$\begin{aligned} \mathbf{n}_p \times (\mathbf{E}_i(P) - \mathbf{E}_e(P)) &= \mathbf{n}_p \times \mathbf{E}^0(P), \\ \mathbf{n}_p \times (\mathbf{H}_i(P) - \mathbf{H}_e(P)) &= \mathbf{n}_p \times \mathbf{H}^0(P), \end{aligned} \quad P \in \partial D \quad (2)$$

and Silver–Muller radiation condition at infinity

$$\lim_{r \rightarrow \infty} \left(\sqrt{\varepsilon_e} \mathbf{E}_e \times \frac{\mathbf{r}}{r} - \sqrt{\mu_e} \mathbf{H}_e \right) = 0, \quad r = |M| \rightarrow \infty. \quad (3)$$

Here $\{\mathbf{E}^0, \mathbf{H}^0\}$ is an exciting field, \mathbf{n}_p is the unit outward normal to ∂D , index e belongs to the external domain D_e , i to domain inside the particle D_i , $\text{Im } \varepsilon_e, \mu_e = 0$, $\text{Im } \varepsilon_i, \mu_i \leq 0$. The boundary value scattering problem is well-known to have the unique solution [14].

One of the most attractive features of DSM consists in flexible choice of DS fields that can be used for approximate solution construction. Additionally, there are no limitations to a choice of support of DS, which should provide fulfilling Maxwell equations, radiation conditions and yield a complete system of DS fields at the obstacle surface [13]. For the oblate obstacles sometimes, it is necessary to find a special DS support. One of the possibilities DSM gives is to deposit DS in a complex plane. Such procedure allows us to limit the DS sequence when $N \rightarrow \infty$. The limitation is very important to provide the stability of the numerical

model based on DSM. Let us shortly describe the procedure of constructing of analytic continuation of DS support to the complex plane with respect to the source's coordinate z_n .

Let us shortly describe the procedure of constructing of an analytic continuation of DS support to the complex plane with respect to the sources coordinate z_n . We will take a halfplane

$$\varphi = \text{const} : \Phi = \{ \eta = (\rho, z) \mid \rho \geq 0, z \in R^1 \}$$

and a complex plane

$$\tilde{\Phi} = \left\{ \tilde{\xi} = \left(\text{Re } \tilde{\xi}, \text{Im } \tilde{\xi} \right) \mid \text{Re } \tilde{\xi}, \text{Im } \tilde{\xi} \in R^1 \right\}.$$

Assume the complex plane $\tilde{\Phi}$ match the real axis in such a way that $\text{Re } \tilde{\xi}$ coincides with z . Now we can represent the system of DS functions using the analytical continuation as follows:

$$\begin{aligned} Y_{mn}(x) &= h_m^2 \left(k_e, R_{\eta\tilde{\xi}} \right) P_m^m \left(\cos \tilde{\theta}_{\tilde{\xi}} \right) \\ &\times \{ 1, \cos m\varphi, \sin m\varphi \}, \quad n, m \in \mathbf{N}, \end{aligned} \quad (4)$$

where

$$\begin{aligned} R_{\eta\tilde{\xi}} &= \rho^2 + \left(z - \tilde{\xi} \right)^2, \quad \text{Re } R \geq 0, \\ \sin \tilde{\theta} &= \frac{\rho}{R_{\eta\tilde{\xi}}}, \quad \cos \tilde{\theta} = \frac{z - \tilde{\xi}}{R_{\eta\tilde{\xi}}}. \end{aligned}$$

Here $R_{\tilde{\xi}}$ is a function of the complex variable $\tilde{\xi}$ and it is chosen so that it represents a branch corresponding to the arithmetical root at the positive part of the real axis.

By definition, the point $\tilde{\xi} \in \tilde{\Phi}$ is called image of the point $\eta \in \Phi$ if $R_{\eta\tilde{\xi}} = 0$.

Lemma 1. For every point $\eta = (\rho, z) \in \Phi$ there are 2 images $\tilde{\xi}^{1,2}$:

$$\text{Re } \tilde{\xi}^{1,2} = z \quad \text{and} \quad \text{Im } \tilde{\xi}^{1,2} = \pm \rho. \quad (5)$$

Proof. The condition $R_{\eta\tilde{\xi}} = 0$ means that

$$\begin{aligned} R_{\eta\tilde{\xi}} &= \left(\rho - \text{Im } \tilde{\xi} \right) \left(\rho + \text{Im } \tilde{\xi} \right) \\ &- 2jm \text{Im } \tilde{\xi} \left(z - \text{Re } \tilde{\xi} \right) + \left(z - \text{Re } \tilde{\xi} \right)^2 = 0, \end{aligned}$$

from the last follows (5). \square

Lemma 2. Let $\eta = (\rho, z)$ be localized outside or on the surface ∂D_i . Then the area of corresponding analytical continuation is a coherent area $D_{\tilde{\xi}} \subset \tilde{\Phi}$, whose boundary coincides with the generatrix \mathbb{L} of revolution $\subset \tilde{\Phi}$.

Proof. The boundary of $D_{\tilde{\xi}}$ is defined by position of η at the object surface. That means that the singularities are distributed in accordance to (5). Those singularities bound the coherent area at the complex plane $\tilde{\Phi}$, whose boundaries coincides with the image of the generatrix \mathbb{L} . It can be shown that $\operatorname{Re} R_{\eta \tilde{\xi}} \geq 0$ for every η localized outside or on the objects surface and $\tilde{\xi} \in D_{\tilde{\xi}}$ [13]. \square

Notation 1. The area where $R_{\eta \tilde{\xi}}$ is an analytical function is symmetric corresponding to the symmetry axis of the scatterer in according to a Schwarz principle.

Lemma 3. Every point $\tilde{\xi}$ in the complex plane $\tilde{\Phi}$ generates the circle of singularities in the real space \mathbf{R}^3 .

Proof. Let us put $\tilde{\xi} \in \tilde{\Phi}$ then (5) provides us a singularity point $\eta = (\rho, z)$, in accordance with (5)

$$\rho = |\operatorname{Im} \tilde{\xi}| \quad \text{and} \quad z = \operatorname{Re} \tilde{\xi}. \quad (6)$$

(6) means that we have singularities distributed on a circle of radius ρ in \mathbf{R}^3 . \square

Lemma 4. Functions (6) with DS situated in $D_{\tilde{\xi}}$ satisfy Maxwell's equations outside the obstacle and radiation conditions at infinity (3).

Proof. The proof is a result of Lemma 1 and asymptotic of spherical Hankel function. \square

Theorem. Let complex coordinates of DS amplitudes $\{\tilde{\xi}\}_{n=1}^{\infty} \in D_{\tilde{\xi}}$ be distributed in accordance with Notation 1 and have at least one condensing point inside $D_{\tilde{\xi}}$, then system (4) is complete and closed in $L^2(\partial D_i)$.

We will consider an axial symmetrical particle, then the system of lowest order multipoles distributed over the axis of symmetry can be applied to construct an approximation solution. As a consequence the surface approximating problem can be reduced to a number of one-dimensional problems enforced at the particle generatrix.

Let the axis of symmetry be the z -axis, DS $\{z_n\}_{n=1}^{\infty}$ distributed over a segment ω_0 of the z -axis, situated inside the particle, which is chosen as a closed multitude with at least one condensing point. Then the follow results are valid [12]:

We will construct the approximate solution by taking into account not only the rotational symmetry of the obstacle, but also the polarization of an external excitation as well.

In case of a P-polarized exciting plane wave the exciting field accepts the following form:

$$\mathbf{E}^0 = (\mathbf{e}_x \cos \theta_0 + \mathbf{e}_z \sin \theta_0) \gamma,$$

$$\mathbf{H}^0 = -\mathbf{e}_y \gamma \cos \theta_0,$$

$$\gamma = \exp\{-jk_c(x \sin \theta_0 - z \cos \theta_0)\},$$

where $k_c = k \sqrt{\epsilon_c \mu_c}$.

To take the polarization of the external excitation into account, we use some linear combination of electrical and magnetic multipoles. For this we need special vector potentials. In case of P-polarization of the plane wave the representation for vector potentials in a cylindrical coordinate system can be represented as:

$$\begin{aligned} \mathbf{A}_{mn}^{1,e,i} &= \{Y_m^{e,i}(\eta, w_n^{e,i}) \cos(m+1)\phi; \\ &\quad - Y_m^{e,i}(\eta, w_n^{e,i}) \sin(m+1)\phi; 0\}, \\ \mathbf{A}_{mn}^{2,e,i} &= \{Y_m^{e,i}(\eta, w_n^{e,i}) \sin(m+1)\phi; \\ &\quad Y_m^{e,i}(\eta, w_n^{e,i}) \cos(m+1)\phi; 0\}. \end{aligned} \quad (7)$$

Vector potentials for vertical dipoles, which are required to provide completeness of the multipoles's system are

$$\mathbf{A}_n^{3,e,i} = \{0, 0, Y_0^{e,i}(\eta, w_n^{e,i})\}.$$

So, the approximate solution taking into account P-polarization of the plane wave, axial symmetry of the particle, can be represented in the form

$$\begin{aligned} \begin{pmatrix} \mathbf{E}_{e,i}^N \\ \mathbf{H}_{e,i}^N \end{pmatrix} &= \sum_{m=0}^M \sum_{n=1}^{N_{e,i}^m} \{p_{mn}^{e,i} D_1 \mathbf{A}_{mn}^{1,e,i} + q_{mn}^{e,i} D_2 \mathbf{A}_{mn}^{2,e,i}\} \\ &\quad + \sum_{n=1}^{N_{e,i}^0} r_n^{e,i} D_1 \mathbf{A}_n^{1,e,i} \end{aligned} \quad (8)$$

here

$$D_1 = \begin{pmatrix} \frac{j}{k_{e,i}\mu_{e,i}} \nabla \times \nabla \\ -\frac{1}{\mu_{e,i}} \nabla \end{pmatrix}, \quad D_2 = \begin{pmatrix} \frac{1}{\epsilon_{e,i}} \nabla \\ \frac{j}{k_{e,i}\mu_{e,i}} \nabla \times \nabla \end{pmatrix}.$$

Then the following result holds:

The approximate solution (8) converges to the exact one under $\{M, N_{e,i}^m\}$ tend to infinity.

In the case of an S-polarized plane wave the exciting field has the form:

$$\begin{aligned} \mathbf{E}^0 &= \mathbf{e}_y \gamma \cos \theta_0, \\ \mathbf{H}^0 &= (\mathbf{e}_x \cos \theta_0 + \mathbf{e}_z \sin \theta_0) \gamma. \end{aligned} \quad (9)$$

The vector potentials corresponding to this case are

$$\begin{aligned} \mathbf{A}_{mn}^{1,e,i} &= \{Y_m^{e,i}(\eta, w_n^{e,i}) \sin(m+1)\phi; \\ &\quad Y_m^{e,i}(\eta, w_n^{e,i}) \cos(m+1)\phi; 0\}, \\ \mathbf{A}_{mn}^{2,e,i} &= \{Y_m^{e,i}(\eta, w_n^{e,i}) \cos(m+1)\phi; \\ &\quad -Y_m^{e,i}(\eta, w_n^{e,i}) \sin(m+1)\phi; 0\}. \end{aligned} \quad (10)$$

Hence the approximate solution can be represented as

$$\begin{pmatrix} \mathbf{E}_{e,i}^N \\ \mathbf{H}_{e,i}^N \end{pmatrix} = \sum_{m=0}^M \sum_{n=1}^{N_{e,i}^m} \{p_{mn}^{e,i} D_1 \mathbf{A}_{mn}^{1,e,i} + q_{mn}^{e,i} D_2 \mathbf{A}_{mn}^{2,e,i}\} + \sum_{n=1}^{N_{e,i}^0} r_n^{e,i} D_2 \mathbf{A}_{0n}^{1,e,i}. \quad (11)$$

The approximate solution (11) corresponding to S-case converges to the exact one under $\{M, N_{e,i}^m\}$ tend to infinity.

3. Numerical algorithm

Let us remind that the approximate solutions for cases of P- (8) and S-polarization (11) satisfy Maxwell's equation (1) and radiating conditions at infinity (3). As the DS are situated on the symmetry axis of the particle, the approximate solution is a finite linear combination of Fourier harmonics with respect to ϕ angle variable. So, at first we resolve the plane wave excitation into a Fourier series with respect to ϕ variable, using the following resolution for the plane wave:

$$\begin{aligned} &\exp\{-jk_e \rho \sin \theta_0 \cos \phi\} \\ &= \sum_{m=0}^{\infty} (2 - \delta_{0m}) (-j)^m J_m(k_e \rho \sin \theta_0) \cos m\phi, \end{aligned} \quad (12)$$

θ_i is the the incident angle of plane wave.

The approximate solution satisfies all the conditions of the original scattering problem, except the transmission conditions. Therefore, the unknown vector of amplitudes of DS

$$\mathbf{p}_m = \{p_{mn}^{e,i}, q_{mn}^{e,i}, r_n^{e,i}\}_{n=1}^{N_{e,i}^m}, \quad (13)$$

where $p_{mn}^{e,i}$ are amplitudes of electric, $q_{mn}^{e,i}$ are the magnetic and $r_n^{e,i}$ are the vector dipoles in representations (8) and (11), is to be determined from the transmission conditions (3). Taking into account, the dependence of the plane wave on the φ angle, we can reduce the surface approximation problem enforced at the particle surface to a sequence of one-dimensional problems at the particle generatrix \mathcal{L} . For solving this problem, we will use the General Matching-Point Technique [15]. At first we choose matching points $\{\eta_l\}_{l=1}^L$ distributed homogeneously over \mathcal{L} . Then by matching the representation for the approximate solution and external excitation at the set of matching points and using the axial symmetry we pass from the surface approximation to the approximation for each Fourier harmonic. As a consequence the unknown vectors of amplitudes \mathbf{p}_m can be found as a pseudosolution of a over-determined system of linear equations [16].

The main feature of the extended DSM algorithm described above to the conventional DSM one [13] consist in deposition of DS in a complex plane.

After DS amplitudes $\{\mathbf{p}_m\}_{m=-1}^M$ have been determined, the far field pattern can be computed [14]:

$$\frac{\mathbf{E}(\mathbf{r})}{|\mathbf{E}^0(\mathbf{r})|} = \frac{\exp(-jk_e r)}{r} \mathbf{F}(\theta, \phi) + o\left(\frac{1}{r}\right), \quad r \rightarrow \infty. \quad (14)$$

The vector $\mathbf{F}(\theta, \phi)$ has two components in the far zone ϕ and θ , so that its components are determined at the unit sphere as

$$\mathbf{F}(\theta, \phi) = \boldsymbol{\theta} \cdot F_\theta(\theta, \phi) + \boldsymbol{\phi} \cdot F_\phi(\theta, \phi). \quad (15)$$

Using asymptotic representation for Y_{mn} for a P-polarized exciting plane wave the far field pattern accepts the form:

$$F_{\theta}^P(\theta, \varphi) = j \sum_{m=0}^M \cos(m+1)\varphi (j \sin \theta)^m \times \sum_{n=1}^{N_c^m} \{p_{mn}^e \cos \theta + q_{mn}^e\} G_n - j \sin \theta \sum_{n=1}^{N_c^0} r_n^e G_n, \quad (16)$$

$$F_{\varphi}^P(\theta, \varphi) = -j \sum_{m=0}^M \sin(m+1)\varphi (j \sin \theta)^m \times \sum_{n=1}^{N_c^m} \{p_{mn}^e + q_{mn}^e \cos \theta\} G_n,$$

where $G_n = \exp\{-jk_e z_n \cos \theta\}$.

Last term in F^P corresponds to vertical dipoles.

For S-polarized excitation the far field components can be written as follows:

$$F_{\theta}^S(\theta, \varphi) = j \sum_{m=0}^M \sin(m+1)\varphi (j \sin \theta)^m \times \sum_{n=1}^{N_c^m} \{p_{mn}^e \cos \theta - q_{mn}^e\} G_n, \\ F_{\varphi}^S(\theta, \varphi) = j \sum_{m=0}^M \cos(m+1)\varphi (j \sin \theta)^m \times \sum_{n=1}^{N_c^m} \{p_{mn}^e - q_{mn}^e \cos \theta\} G_n + j \sin \theta \sum_{n=1}^{N_c^0} r_n^e G_n. \quad (17)$$

4. Results and discussion

In this section, we will discuss some numerical results. The aim of the investigation was to find out if the commonly used shape models for erythrocyte modeling, like oblate spheroid and disk-sphere, give acceptable results in comparison with the rigorous shape. We investigated differential scattering cross-section, which can be calculated analytically via the components of the far field pattern given in (16) and (17) respectively:

$$DSC^{P,S} = |F_{\theta}^{P,S}(\theta, \varphi)|^2 + |F_{\varphi}^{P,S}(\theta, \varphi)|^2. \quad (18)$$

As external media for our erythrocyte we have chosen water, as its refractive index is very close to plasma and is often used for modeling. As incident wavelength we took $\lambda = 476$ nm, that corresponds $\lambda = 632.8$ nm in water. The refractive index of erythrocyte with respect to the water: $n = 1.058$, diameter $D = 6.3$ μm . For oblate spheroid and disk-sphere, we took the same diameter and aspect ratio of 1:4 which is widely used in investigations. At first we would like to present some results for the rigorous shape [2] which can be described by:

$$z^2 = \left(\frac{0.86d}{2}\right)^2 \left[1 - \left(\frac{2x}{d}\right)^2\right] 0.01384083 + 0.2842917 \left(\frac{2x}{d}\right)^2 + 0.01306932 \left(\frac{2x}{d}\right)^4. \quad (19)$$

In Fig. 1, the real human erythrocyte shape, disk-sphere model and oblate spheroid model are shown in 3D-view and as 2D cut. In Fig. 2, the computational results for the real erythrocyte shape with the incident angle $\theta_i = 150^\circ$ for P and S polarized excitation are presented. In Fig. 3, results are shown for incident angles $\theta_i = 120^\circ$ and $\theta_i = 180^\circ$. From Figs. 2 and 3, one can see that varying of the incident angle does not only change the position of the main peaks, but also the shape of graphs for both polarizations.

In Fig. 4, results of comparison of three different shapes are shown for $\theta_i = 135^\circ$ and P-polarized light. In Fig. 5 similar results are shown for $\theta_i = 180^\circ$. From Figs. 4 and 5, it seems that the model of disk-sphere is more acceptable to approximate real erythrocyte shape. So we will investigate in more details the scattering angle band $10\text{--}50^\circ$ which includes the band of most interest in cytometry: $15\text{--}40^\circ$. Problems can appear due to a shift of the position of the main peak under different incident angles, because one can see from Figs. 4 and 5 that under different incident angles different part of scattering diagram appears in angle band $10\text{--}50^\circ$.

In Figs. 6–9, results of comparing different shapes for different incident angles are shown. In Figs. 6 and 7, results for incidence $\theta_i = 180^\circ$ are presented P and S-polarized light, respectively, for the chosen band of scattering angles. From comparison one can see that for both P and

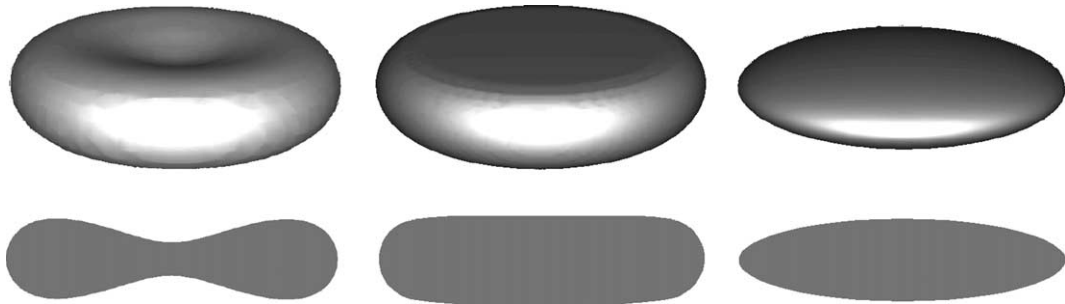


Fig. 1. Shape models 3D-view (above) and 2D-cut (below): real human erythrocyte (left), disc-sphere (middle), oblate spheroid (right).

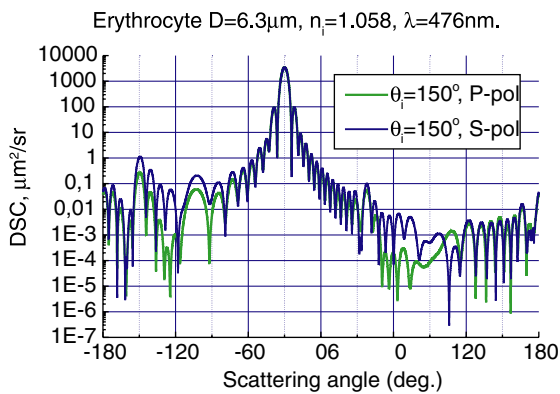


Fig. 2. Dependence of DSC from scattering angle θ in the plane of incidence $\varphi = 0$, from rigorous erythrocyte shape for the incident angle of plane wave $\theta_i = 150^\circ$, P and S polarized light.

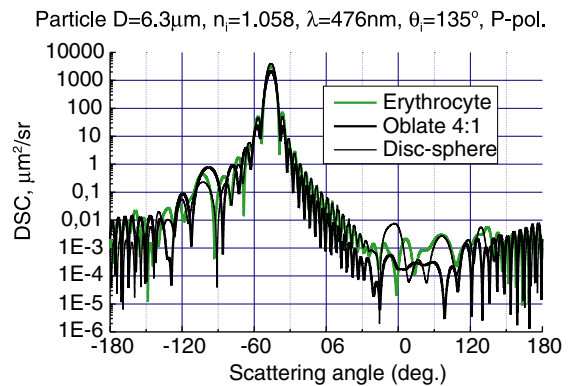


Fig. 4. DSC versus scattering angle for P-polarization from different shape models for $\theta_i = 135^\circ$.

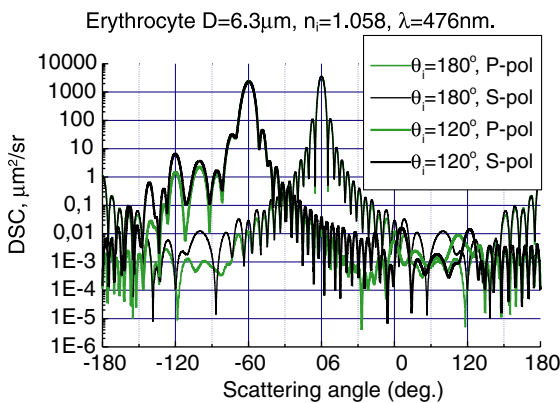


Fig. 3. Dependence of DSC from scattering angle θ in the plane of incidence $\varphi = 0$, from rigorous erythrocyte shape for $\theta_i = 120^\circ$ and $\theta_i = 180^\circ$, P and S polarized light.

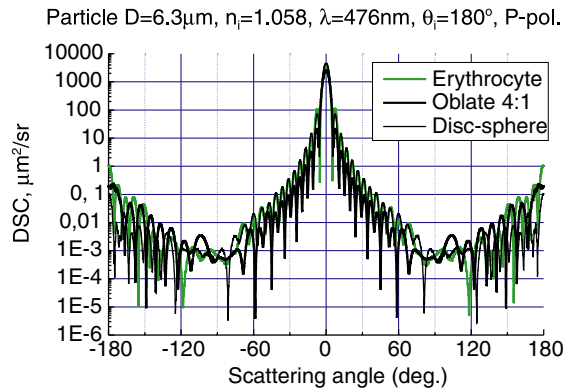


Fig. 5. DSC versus scattering angle for P-polarization from different shape models for $\theta_i = 180^\circ$.

S-polarized light the model of disk-sphere shows reasonable agreement with the rigorous shape. In Fig. 8, similar results are shown for incidence

$\theta_i = 150^\circ$, P polarization, here the model of disk-sphere also fits good with rigorous one. And in Fig. 9 similar results for P polarization are shown for incidence $\theta_i = 135^\circ$. Here the difference

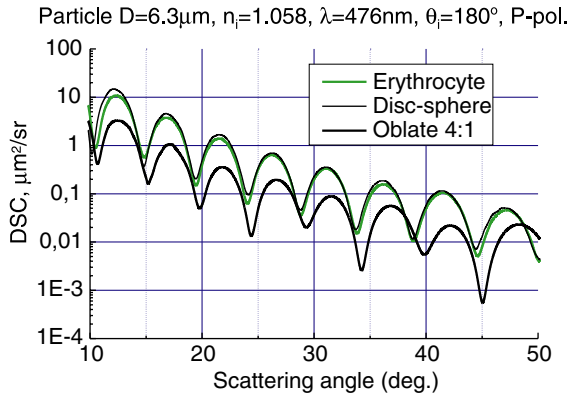


Fig. 6. DSC versus scattering angle for P-polarization from different shape models for $\theta_i = 180^\circ$ in scattering angle band 10–50°.

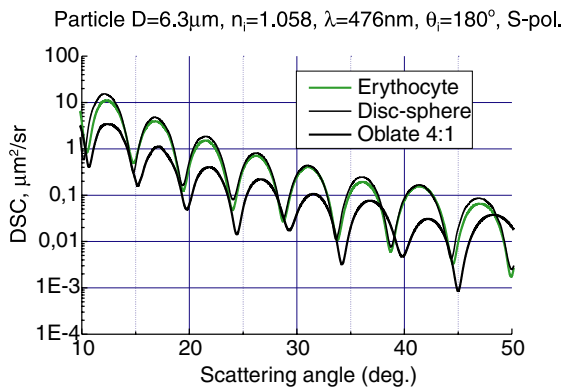


Fig. 7. DSC versus scattering angle for S-polarization from different shape models for $\theta_i = 180^\circ$ in scattering angle band 10–50°.

between disk-sphere is more obvious, but still better than between rigorous shape and oblate spheroid. With decreasing incident angle the difference between the models becomes more obvious, but the shape of disk-sphere shows better agreement to the real shape. This fact allows us to conclude that in theoretical investigations it is better to use the rigorous erythrocyte shape, but in cases where some approximations are necessary, for example to reduce time of calculations or use more powerful methods such as T-matrix method which are not able to deal with concavities, it seems to be more reasonable to use the model of disk-sphere instead of widely used spheroid model.

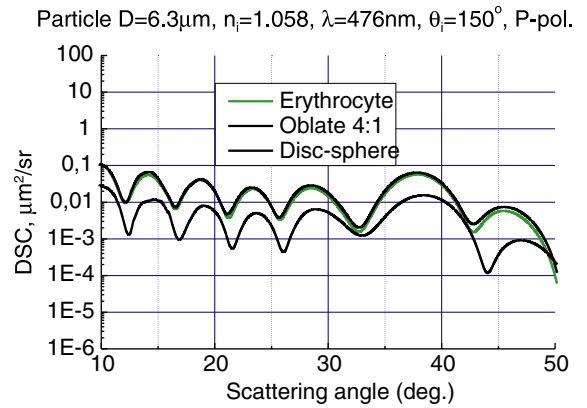


Fig. 8. DSC versus scattering angle for P-polarization from different shape models for $\theta_i = 150^\circ$ in scattering angle band 10–50°.

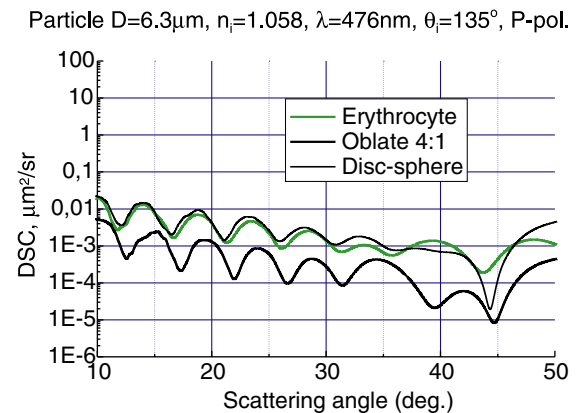


Fig. 9. DSC versus scattering angle for P-polarization from different shape models for $\theta_i = 135^\circ$ in scattering angle band 10–50°.

In conclusion we would like to mention that the most time-consuming calculation for rigorous erythrocyte shape (for all the incident angles and polarizations at once) took less than a minute for Pentium IV 1600 Hz with 512 Mb RAM. The most advanced DDA algorithms need at least several minutes for every incident angle. The important feature of DSM consist in possibility to calculate an a-posterior residual of the obtained results [13]. It is also possible to reduce the residual by choosing number of discrete sources N and matching points L . In presented results the residual does not exceed 0.1% further decreasing of the residual

is useless, because the results does not change with residual reduction.

5. Conclusions

A renewed algorithm of the DSM was applied to model light scattering by the human red blood cell. The main differences of the extended DSM scheme to the conventional DSM one [13] are: different numbers of DS are used for the representation of the scattered field outside and total field inside the particle, and the number of DS depends on the rank of Fourier harmonics. This means that for higher harmonics the lower numbers of multipoles are used. Such novations allow using a lower number of DS and increasing the accuracy of harmonics approximation. Additionally we should mention that the modeling of exact erythrocyte shape requires 45 Fourier harmonics, which has never been achieved before. Such approach enables to acquire a more accurate simulation results, provides a monotone decrease of the surface residual and to reduce the demand on computer resources for a large particles, like erythrocyte, compared to the conventional DSM model. Applicability of the renewed algorithm is checked by calculation of the surface residual.

The results obtained on the base of the new scheme allows us to recommend using the less popular model of disk-sphere instead of the spheroid model in cases where such approximation is still needed.

Acknowledgments

We gratefully acknowledge financial support of this research by Deutsche Forschungsgemeinschaft

(DFG) and Russian Foundation for Basic Research (RFBR).

References

- [1] K.A. Sem'yanov, P.A. Tarasov, J.T. Soini, A.K. Petrov, V.P. Maltsev, *Appl. Opt.* 39 (31) (2000) 5884.
- [2] N. Schvalov, J.T. Soini, A.V. Chernyshev, P.A. Tarasov, E. Soini, V.P. Maltsev, *Appl. Opt.* 38 (1) (1998) 230.
- [3] V. Tuchin (Ed.), *Tissue Optics: Light Scattering Methods and Instruments for Medical Diagnosis*, SPIE Press, 2000.
- [4] A. Roggan, et al., *J Biomed. Opt.* 4 (1999) 36.
- [5] V.N. Lopatin, N.V. Shepelevich, *Opt. Spectrosc.* 81 (1996) 103.
- [6] G.J. Streekstra, A.G. Hoekstra, E. Nijhof, R.M. Heethaar, *Appl. Opt.* 32 (1993) 2266.
- [7] M. Hammer, D. Schweitzer, B. Michel, E. Thamm, A. Kolb, *Appl. Opt.* 37 (31) (1998) 7410.
- [8] N.K. Uzunoglu, D. Yova, G.S. Stamatakos, *J. Biomed. Opt.* 2 (3) (1997) 310.
- [9] A.M.K. Nilsson, P. Alsolm, A. Karlsson, S. Andersson-Engels, *Appl. Opt.* 37 (1998) 2735.
- [10] J. Neukammer, G. Gohlke, A. Höpe, T. Wessel, H. Rinneberg, *Appl. Opt.* 42 (31) (2003) 6388.
- [11] S.V. Tsinopoulos, D. Polyzos, *Appl. Opt.* 38 (25) (1999) 5499.
- [12] A. Doicu, Y. Eremin, T. Wriedt, *Acoustic and Electromagnetic Scattering Analysis using Discrete Source*, Academic Press, San Diego, 2000.
- [13] Y. Eremin, N. Orlov, A. Sveshnikov, *Models of electromagnetic scattering problems based on discrete sources method*, in: t. wriedt (Ed.), *Generalizes Multipole Techniques for Electromagnetic and Light Scattering*, Elsevier Science, Amsterdam, 1999, p. 39.
- [14] D. Colton, R. Kress, *Inverse Acoustic and Electromagnetic Scattering Theory*, Springer, Berlin, 1992.
- [15] V. Voevodyn, A. Kuznetsov, *Matrices and calculations* (Moscow, Science, 1982) (in Russian).
- [16] E. Eremina, Y. Eremin, T. Wriedt, *J. Mod. Opt.* 51 (3) (2004) 423.